Uranyl Photoprobing of Nonbent A/T- and Bent A-Tracts. A Difference of Flexibility?†

Niels Erik Møllegaard, Søren Lindemose, and Peter E. Nielsen*

Department of Medical Biochemistry and Genetics, The Panum Institute, University of Copenhagen Blegdamsvej 3c, 2200 Copenhagen N, Denmark

Received February 4, 2005; Revised Manuscript Received April 1, 2005

ABSTRACT: In this study, we have systematically compared the uranyl photocleavage of a range of bent A-tracts and nonbent TA-tracts as well as interrupted A-tracts. We demonstrate that uranyl photocleavage of A-tracts and TA-tracts is almost identical, indicating a very similar minor groove conformation. Furthermore, a 10 base pair A-tract is divided into two independent tracts by an intervening TA or GC step. Uranyl probing also clearly distinguishes the bent A_4T_4 and the nonbent T_4A_4 sequences as adopting different structures, and our interpretation of the data is consistent with a structure for the bent A_4T_4 sequence that resembles a continuous A-tract, whereas the nonbent T_4A_4 sequences are closer to two independent and opposite A-tracts that cancel each other in terms of macroscopic bending. Finally, we also note that even single TA and TAT steps are highly sensitive to uranyl photocleavage and propose that in addition to avarage minor groove width, uranyl also senses DNA helix flexibility/deformability. Thus, the structural difference of TA-tracts and A-tracts may to a large extent reflect a difference in flexibility, and DNA curvature may consequently require a rigid narrow minor groove conformation that creates distinct A-tract−B-DNA junctions as the predominant cause of the bending.

Double-stranded DNA containing A-tracts of at least four consecutive A/T base pairs, positioned in phase with the helical pitch (approximately 10.5 base pairs) exhibits macroscopic curvature, and several models have been proposed to explain this phenomenon (*1*). One model suggests that DNA curvature results from the additive effect of unique ApA wedges in A-tracts produced by roll angles at these steps (*2*, *3*). A related model claims that individual rolls characterize all base pairs in DNA and that solely ApA steps possess no roll. According to this model, curvature is an inherent property of random sequence B DNA and therefore occurs between the A-tracts, which are themselves straight (*4*, *5*). A third model suggests that adenine tracts have a unique structure, which is formed by negative inclination between base pairs within the A-tract. This model is known as the "junction model" because curvature (or rather kinking) is proposed to take place where the normal B-DNA conformation of random sequences and the A-tract conformation meet each other (*6*−*8*).

Results obtained from A-tract crystal structures compared to solution studies (gel mobility, chemical probing, and NMR) have led to somewhat conflicting conclusions about the origin of DNA curvature. Nevertheless, several features are shared by A-tract crystal structures and structures inferred from solution experiments, such as narrow minor groove, propeller twisting, and hydration spines. A number of experiments have demonstrated that the minor groove in an A-tract is narrowing from the 5′ end toward the 3′ end. In longer A-tracts, the minor groove is narrowing over the first three to four base pairs from the 5′ end followed by a minor groove width, which remains constant throughout the A-tract, toward the 3′ end (*9*−*13*). Crystal structure analysis has shown that compression of the minor groove is a result of a substantial propeller twisting in the AT base pairs of A-tracts (*10*, *14*, *15*). Furthermore, a narrow minor groove is required for optimal interactions between bases and water, forming a characteristic spine of hydration in the minor groove of A-tracts (*16*, *17*).

DNA curvature is critically dependent on the presence of a pure A-tract because 5′-TA steps or G/C bases within A-tracts destroy the A-tract structure (*18*−*20*). Likewise, 5′-TA steps and GC sequences disrupt the spine of hydration possibly because of the reduced propeller twist in these base pairs (*15*).

Although, the narrow minor groove of A-tracts is indisputable, narrowing of the minor groove along A-tracts is hardly per se responsible for DNA curvature. For instance, inosine tracts repeated in phase with the helical screw of the DNA helix do not induce a macroscopic curvature of the DNA, although the inosine tracts do possess a narrow minor groove according to chemical probing (*21*). Furthermore, crystal structures of $CGC(AT)_3GCG$ and $CGCG(AT)_2CGCG$ sequences show narrow minor grooves comparable to pure A-tracts, although these sequences do not induce macroscopic DNA bending (*22*). In addition, NMR studies of AAAATTTT, TTTTAAAA, and ATATATAT duplexes suggest that a narrow minor groove is present for all sequences (*23*). Finally, uranyl probing of $(T/A)_4$ regions produces a similar pattern characteristic of a narrow minor groove for all (T/

† This work was supported by The Lundbeck Foundation, The Novo-Nordisk Foundation, The Danish National Research Foundation, and the Augustinus Foundation.

* To whom correspondence should be addressed. Telephone: +45 35327762. Fax: +45 35396042. E-mail: pen@imbg.ku.dk.

10.1021/bi0502083 CCC: $30.25
Published on Web 05/06/2005

$A)_4$ combinations (*24*). Thus, A/T-tracts appear to have a narrow minor groove structure very similar to that of A-tracts.

Uranyl (UO_2^{2+}) binds to the phosphates of the DNA backbone and induces cleavage of the backbone by oxidation of proximal deoxyriboses upon irradiation. Uranyl photocleavage has within recent years been used for studying protein−DNA interactions, drug−DNA interactions, and the interactions of metal ions with nucleic acids (e.g., see refs *25*−*29*). Most interestingly, uranyl photocleavage of DNA at slightly acidic pH (below 6.5) shows high efficiency at A/T-rich regions and low efficiency at G/C-rich regions (*30*). Furthermore, the uranyl hypersensitivity at $(A/T)_4$ sequences is increasing from the 5′ end toward the 3′ end (*24*), and this is consistent with a progressive narrowing of the minor groove from the 5′ toward the 3′ end. Many lines of evidence indicate a direct correlation between uranyl photocleavage efficiency and minor groove width and/or electronegative potential (*24*, *28*, *31*, *32*). It may indeed be that the uranyl ion predominantly senses the electronegative potential of the groove, which is especially large in regions of narrow minor grooves, where the phosphates of the two strands are closer to each other (*30*).

In the present work, we have used uranyl probing for studying the properties of A/T-rich sequences consisting of pure A-tracts and sequences containing TA steps to further understand the relation between A-tract structure, minor groove width, and DNA curvature.

MATERIALS AND METHODS

Plasmids. The plasmid pA_{1-8} was constructed by cloning a 75 base pair fragment containing adenine tracts with one to eight adenines separated by CGGC into the *Bam*HI site of pUC 19. Likewise, pTA_{1-8} was constructed by cloning a 75 base pair fragment containing mixed A−T-tracts of one to eight A/T basepairs in the *Bam*HI site of pUC 19.

The plasmids $pT_{10}A_{10}$, pA_9GT_9C, and pA_9T were constructed by cloning a 5′-AAAAAAAAAA-3′, a 5-AAAAGAAAAA-3′, and a 5′AAAATAAAA-3′ sequence in the *Bam*HI site of the bluescript KS vector. The two plasmids pA_4T_4 and pT_4A_4 containing four inserts of the AAAATTTTGC and TTTTAAAAGC sequences were constructed by cloning self-complementary oligonucleotides of 52 base pairs in the *Bam*HI site of pUC 19.

Purification of DNA Fragments. The plasmids were cleaved by restriction enzymes using standard techniques and ^{32}P labeled at either the 3′ end using $\alpha[^{32}P]$-dATP (Amersham) and the klenow fragment from DNA polymerase I (Gibco, BRL) or the 5′ end using $\gamma[^{32}P]$-ATP (Amersham) and polynucleotide kinase (Gibco, BRL) labeling of dephosphorylated DNA ends.

DNA fragments containing the relevant sequences were isolated on 5% native polyacrylamide gels and eluted from the gel slice by diffusion in 90 mM Tris-borate and 1 mM EDTA at pH 7.5.

Uranyl Photocleavage. The purified DNA fragments were subject to uranyl photocleavage in a volume of 100 μL containing 50 mM NaAc at pH 6.2 and 1 mM uranyl nitrate. The samples were irradiated in open tubes placed just below a 40W/03 Phillips fluorescent light tube with maximum emission at 420 nm. After 20 min of irradiation, NaAc at pH 4.5 was added to a final concentration of 0.2 M together with 2.5 volumes of ethanol. The tubes were placed on ice for 15 min and thereafter centrifuged for 15 min. The dried pellet was dissolved in 6 μL of formamide, 90 mM Tris-borate, and 1 mM EDTA at pH 8.3 containing xylene cyanol and bromophenol blue and the samples were heated at 90 °C before loading 2 μL onto a 10% denaturing polyacrylamide gel (19:1 acrylamide/methylenebisacrylamide). The autoradiograms were obtained by overnight exposure using intensifying screens.

Data Analysis. Autoradiographs of uranyl cleavage digestion patterns were scanned using a Molecular Dynamics computing densitometer. Control lanes from samples without uranyl treatment were blank, showing no background cleavage bands. To quantify the gels, baseline-corrected scans were analyzed by integrating all of the densities between two selected boundaries using ImageQuant software version 5.1. The area under the peak was integrated by simple addition of the pixels under the curve. Cleavage data are presented as either autoradiographs and/or densitometric scans of the autoradiographs.

Calculation of Uranyl Binding Based on Cleavage Data. Uranyl binding to a specific phosphate induces equal cleavage at the sugar (and thus nucleobase) at both the 3′ as well as 5′ side (*31*). Therefore, the binding of uranyl to a specific phosphate can mathematically be derived from the cleavage results as follows.

If we consider a DNA backbone (S = sugar, P = phosphate) and $S^1-P^1-S^2-P^2-S^3-P^3-S^4-P^4$ ..., S^n-P^n, where X_n is the binding of uranyl to phosphate n and Y_n is the cleavage at sugar n, it follows from experimental evidence that (*31*)

$$Y_n = 0.5(X_n + X_{n-1})$$

Consequently, X_n is defined by two equations: $0.5X_n = Y_n - 0.5X_{n-1}$ and $0.5X_n = Y_{n+1} - 0.5X_{n+1}$.

Therefore, by addition

$$X_n = Y_n + Y_{n+1} - 0.5(X_{n-1} + X_{n+1})$$

By iterative substitution in this equation, one obtains the general calculation of X_n based on all cleavage intensities

$$X_n = Y_n + Y_{n+1} - 0.5(Y_{n-1} + Y_{n+2}) + 0.25(Y_{n-2} + Y_{n+3}) - 0.125(Y_{n-3} + Y_{n+4}) + 0.0625(Y_{n-4} + Y_{n+5}) \ldots$$

For the calculations of uranyl binding efficiencies (to phosphate X_n), we used up to eight cleavage intensities (from Y_{n-3} to Y_{n+4}).

Ligation Ladders. DNA oligonucleotides were purchased from DNA Technology A/S, Denmark. Single-stranded oligonucleotides were phosphorylated with $\gamma[^{32}P]$-ATP and T_4 polynucleotide kinase (Fermentas) according to the recommendations of the manufacturer. Then, equal amounts (1 μg) of complementary ^{32}P-labeled oligonucleotides were mixed and heated to 90 °C for 2 min and cooled gradually to room temperature (23 °C). The annealed oligonucleotides were then assembled into ligation reactions containing 800 units of T4 DNA ligase (Fermentas) and incubated at 4 °C for 12−14 h. After incubation, the samples were analyzed by polyacrylamide gel electrophoresis on native gels. Autoradiographs were used to determine the relative mobilities of DNA fragments (A_4N_6, 5′-GGCCAAAACG;

A_8N_2, 5′-CCAAAAAAAA; A_4T_4, 5′-AAAATTTTGC; T_4A_4, 5′-TTTTAAAAGC; TATAT, 5′-CCGCTATATG) compared to a standard sequence (5′-CCGTGTCTG).

RESULTS

Uranyl Cleavage of A-Tracts Is Consistent with a Unique DNA Structure with a Minor Groove Narrowing from the 5′ End toward the 3′ End. In the first part of this study, the structure of A-tracts with exclusively AA steps was examined (these are referred to as pure A-tracts). For this purpose, a plasmid (pA_{1-8}) containing sequences of one to eight adenines each separated by a CGGC sequence was constructed. Thus, seven A-tracts are analyzed (A_2, A_3, A_4, A_5, A_6, A_7, and A_8) of which A_2 and A_3 are not expected to adopt the unique A-tract structure essential for DNA bending.

The analysis is done by measuring the uranyl photocleavage at individual phosphates of ^{32}P-end-labeled DNA fragments under conditions that result in clear sequence-dependent cleavage modulation (pH ≤ 6.5) (*30*). Typical autoradiograms displaying uranyl cleavage of a DNA fragment from pA_{1-8} are shown in Figure 1A and the corresponding scans in Figure 1B. Both the A-rich and the T-rich strands of the DNA were analyzed, and for the T strand, this was done from the 3′ end as well as from the 5′ end. The results demonstrate that uranyl photocleavage is highly variable along the DNA fragment and that uranyl cleavage is strongest in regions containing four or more adenines/thymidines in a row and weakest in the intervening G/C sequences. Characteristically, the cleavage intensity of the A-rich strand builds up from the 5′ end of each A-tract within four bases and thereafter remains practically constant toward the 3′ end (Figure 1B, upper scan). The cleavage pattern of the T-rich strand is somewhat different. In this case, cleavage intensity builds up from the 3′ end as well as from the 5′ end and the constantly cleaved positions are found in the middle of the T-tract (middle and lower scans).

If uranyl photocleavage does indeed probe the width of the minor groove as previously suggested (*30*), a correlation of the cleavage at the two phosphates facing each other at the shortest distance across the groove [i.e., the *n*th phosphate on the upper A-rich strand and the (n − 2)th (or the (n − 3)rd) phosphate on the lower T-rich strand] is expected. As indicated earlier for other A/T sequences, this is also the case for the A-tract sequences of pA_{1-8} (Figure 1C). The mechanism of uranyl cleavage has to be considered when a quantitative interpretation of the cleavage intensities is attempted. It was previously found that binding to a specific phosphate induces approximately equal cleavage at the sugar (and thus nucleobase) at both the 3′ as well as the 5′ side proximal to the phosphate (*31*). Therefore, the binding of uranyl to a specific phosphate can mathematically be derived from the cleavage results (see the Materials and Methods). This approach clearly demonstrates that relative binding is correlated between the *n*th position on the upper strand and the (n − 2)th position on the lower strand, which emphasizes a mechanism involving uranyl cleavage/binding via the minor groove as well as a reverse correlation between the intensity of uranyl photocleavage and minor groove width (*30*). The relative minor groove width deduced from this analysis is illustrated by lines between the n and (n − 2)th positions below the histograms (Figure 1C). In principle, it should be possible by calibrating these results with X-ray crystallography structural data to derive absolute values for the minor groove width from uranyl cleavage results, but our data do not allow for that at the present stage.

The cleavage pattern supports the existence of a unique A-tract structure, where the minor grove is gradually narrowing from the 5′ end toward the 3′ end, reaching a minimum approximately at adenine number four from the 5′ end as previously concluded from other methods (*13*, *33*−*35*). In addition, the result suggests that the absolute minor groove width of A-tracts is dependent upon the number of A/T base pairs in the tracts. As an illustrative example, the minor groove width is narrower in the A_8-tract than in the A_4-tract. This is consistent with NMR experiments and lifetime measurements showing that the distance across the minor groove varies, with the number of A/T base pairs being shorter in longer A-tracts (*10*, *12*, *13*).

A Single G/C Base Pair Interrupts the A-Tract Conformation. A detailed analysis of the sequence requirement for DNA curvature has shown that an intact A-tract structure is crucial (*6*, *8*, *36*). We chose to analyze uranyl cleavage of an A-tract interrupted by a single G/C base pair. As representative of a pure A-tract, an T_{10}/A_{10} sequence included in plasmid $pT_{10}A_{10}$ was used. For comparison, an A_5GA_4 sequence included in plasmid pA_9GT_9C was used to study the effect of a G/C base pair. As expected from the results with A_8 inserts presented above, uranyl cleavage increases from the 5′ end toward the 3′ end of the A-tract containing 10 adenines, reaching a maximum at adenine number five from the 5′ end and at thymidine number six from the 5′ end (Figure 2A). Notably, the uranyl cleavage pattern is completely changed if a single A/T base pair is substituted with a G/C base pair in the center of the sequence as illustrated by uranyl cleavage of the A_4GA_5/T_4CT_5 sequence (lower scan of Figure 2A). Cleavage increases from the 5′ end toward the 3′ end of the four thymidines, reaching a maximum at the most 3′ thymidine. The presence of the C results in a dramatic reduction in reactivity at the two thymines following the C, but uranyl reactivity increases again from the 5′ end toward the 3′ end of the following five thymidines. The cleavage pattern is analogous in the A-rich sequence exhibiting an increased uranyl cleavage from the 5′ end toward the 3′ end of both of the two A-tracts interrupted by a guanine. It is also noted that the cleavage is much stronger in the T-rich sequence than in the A-rich sequence. The quantified results shown in Figure 2B again stress a good correlation between cleavage at the *n*th and the (n − 2)th nucleotide. Thus, the presence of a guanine in the center of the long A-tract effectively interrupts the progressive build up of a long A-tract structure with narrowing of the minor groove toward the 3′ end. Instead, two independent A-tracts are generated both with narrowing of the minor groove from the 5′ end toward the 3′ end.

A Single TA Step within an A-Tract Affects Minor Groove Width. A single TA step is inherently more flexible than all other base pair steps and is able to adopt large roll, twist, and slide values. Accordingly, introduction of a TA step within an A-tract causes a disruption of the A-tract conformation, which eliminates DNA curvature (*37*). Uranyl cleavage of a sequence from pA_9T containing a row of adenines interrupted by a single TA step is presented in Figure 3A. The sequence behaves essentially as the G/C

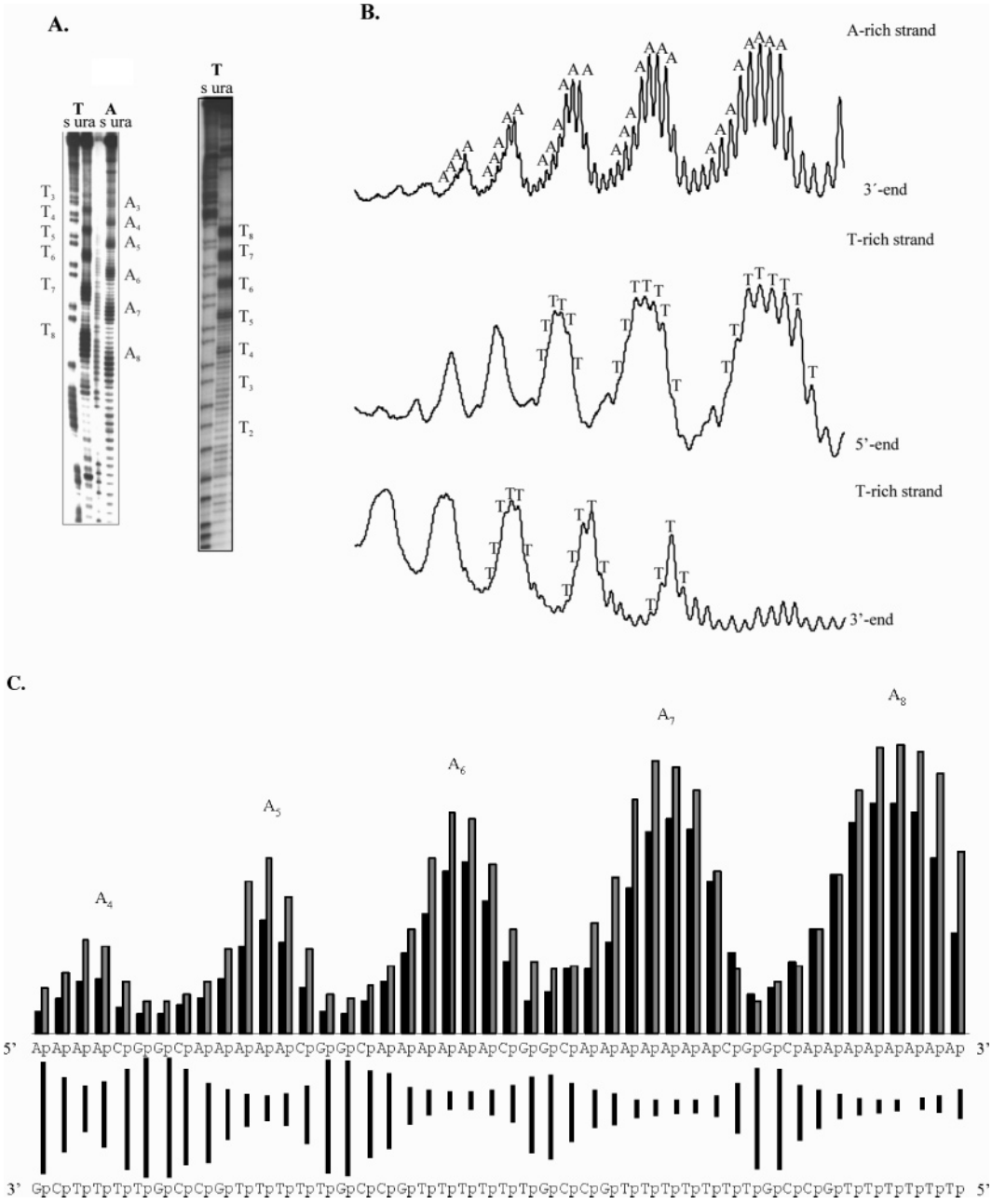

FIGURE 1: (A) Left autoradiogram shows uranyl cleavage of the two strands of the A-tracts containing DNA fragments from pA_{1-8}. The A-rich strand ("A") is labeled in the 3′ end and the T-rich strand ("T") is labeled in the 5′ end. The right autoradiogram shows the T-rich strand labeled in the 3′ end. s denotes A/G sequence reactions, and ura denotes uranyl cleavage. (B) Corresponding scans. Upper scan represents the 3′-labeled A-rich strand, and the middle and lower scans represent the 5′- and 3′-labeled T-rich strands shown in the autoradiograms. The A- and T-rich sequences are indicated along the autoradiograms and in the scans. (C) Correlation between calculated uranyl phosphate binding and minor groove width in the A-tract sequences. The histogram shows calculated uranyl binding to the *n*th (black bars) (using Y_n and Y_{n+1}) and the $(n - 2)$th (gray bars) phosphates. Uranyl binding is correlated with the width of the minor groove below the histogram where the *n*th and the $(n - 2)$th positions are aligned across each other. The lengths of the black lines between the sequences correspond to relative minor groove width calculated as the reciprocal value of the *n* plus $n - 2$ combined binding efficiency. Because the results for the A and T strands were obtained from different experiments, the absolute cleavage/binding efficiencies cannot be compared accurately. Numbers of adenines in each tract are denoted above the histogram.

interrupted long A-tract discussed above. However, the TA step clearly has a lesser effect on uranyl cleavage as compared to the effect of a G/C base pair (compare Figure 2B with Figure 3B). Our quantification indicates that the minor groove around the G/C base pair in the center of a long A-tract sequence returns to the width as present in the surrounding GC sequences, whereas the minor groove width in the region of the TA step is still more narrow than in the surrounding sequences (Figure 3B). The detrimental effect on curvature by the presence of a TA step within A-tracts has previously been ascribed to a local widening of the minor groove, and our results are in agreement with this conclusion (*38*−*42*).

Uranyl Cleavage of 5′-TA-Containing Sequences Exhibits Minor Groove Narrowing from the 5′ End toward the 3′ End. Previous experiments have shown that uranyl reactivity is very strong not only in pure A-tracts but also in A/T regions in general (*24*). We have addressed this feature of uranyl

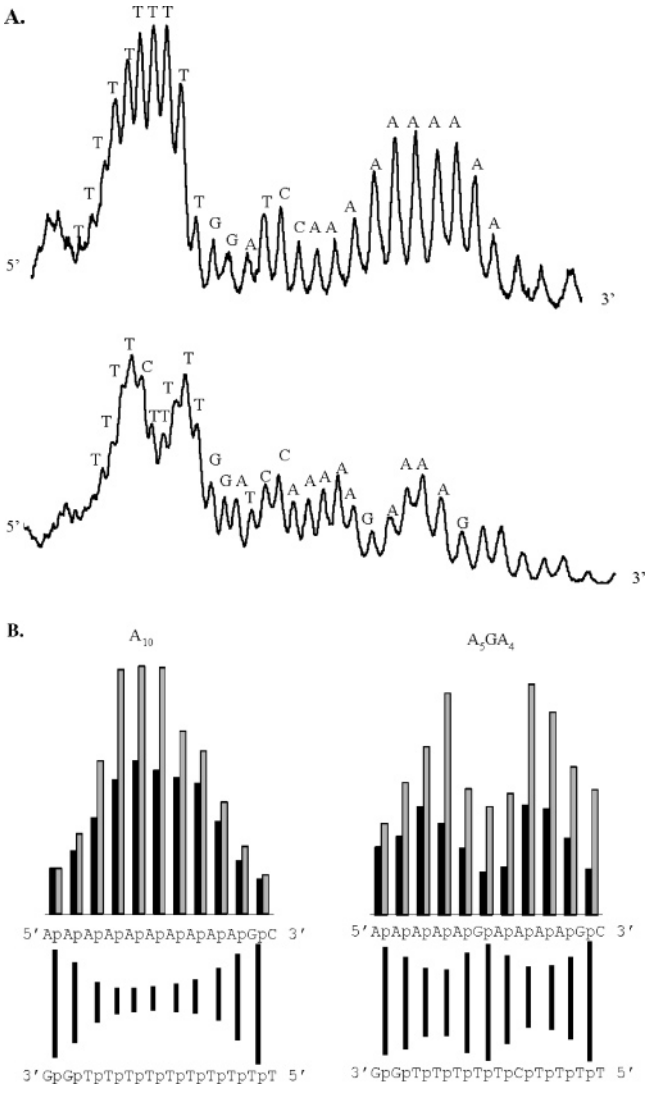

FIGURE 2: Effect of a G/C base pair within A-tracts. (A) Upper scan corresponds to uranyl cleavage of the A_{10}/T_{10} sequence, and the lower scan corresponds to the A_5GA_4/T_5CT_4 sequence. (B) Correlation between calculated uranyl binding and minor groove width in the A_{10}/T_{10} and A_5GA_4/T_5CT_4 sequences. The histogram shows calculated phosphate binding to the *n*th (black bars) (using Y_n to Y_{n-3} and Y_{n+1} to Y_{n+4}) and the $(n-2)$th (gray bars) phosphates. Uranyl binding is correlated with the width of the minor groove below the histogram as in Figure 1. Because the results for the A and T strands were obtained from different experiments, the absolute cleavage/binding efficiencies cannot be compared accurately.

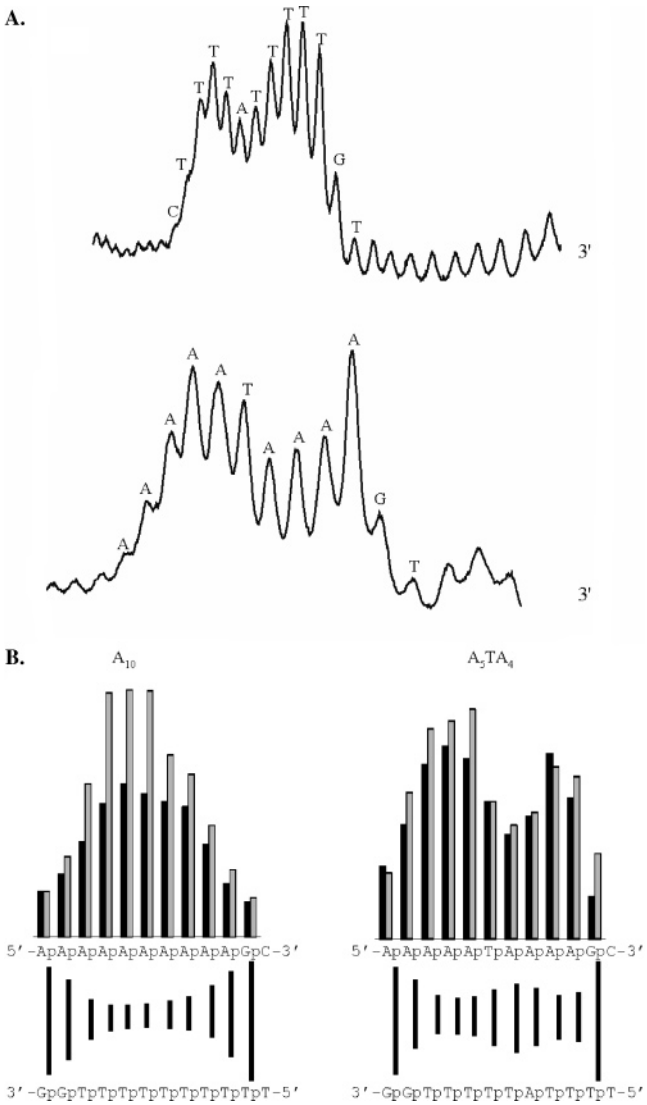

FIGURE 3: Effect of a 5′-TA step within A-tracts. (A) Result of uranyl cleavage of an A_5TA_4/T_5AT_4 sequence is represented by scans. (B) Correlation between calculated uranyl phosphate binding and minor groove width in the A_{10}/T_{10} and A_5TA_4/T_5AT_4 sequences. The histogram shows calculated uranyl binding to the *n*th (black bars) (using Y_n and Y_{n+1}) and the $(n-2)$th (gray bars) phosphates. Uranyl binding is correlated with the width of the minor groove as in Figure 1. The results for the A and T strands were obtained from cleavage on the same DNA fragment experiments, and therefore, the absolute cleavage/binding efficiencies can be compared directly.

cleavage in more detail by analyzing a sequence with 5′-TA steps building up from a single TA sequence to a TATA-TATA sequence. The A/T-rich regions are separated by a CGGC sequence, which makes possible a direct comparison with uranyl cleavage of the pure A-tract sequences, analyzed above.

However, again, it is shown that uranyl hypersensitivity is restricted to regions containing A/T base pairs. Uranyl cleavage of the two strands is characterized by weak cleavage in the G/C sequences and in the 5′ end of the A/T sequences (parts A and B of Figure 4). Through each A/T sequence, cleavage is progressively increasing toward the 3′ end reaching a maximum around A/T base pair number four from the 5′ end. When the results are interpreted in terms of minor groove width, the cleavage of the A/T-rich sequences is clearly characterized by a pattern consistent with narrowing of the minor groove toward the middle of the sequence quite analogously to the behavior of pure A-tracts (Figure 4B).

As observed for the pure A-tracts, cleavage in longer A/T-tracts is also stronger than in shorter A/T-tracts, which is consistent with a more narrow minor groove in the longer AT sequences as previously suggested by others (*12*, *13*).

Thus, the striking similarity between the cleavage pattern of the pure A-tract sequence and the TA sequences points to a very similar minor groove width in pure A-tracts and in alternating TA sequences (compare Figures 1C and 4B). Interestingly, however, even the short TA and TAT steps also induce some uranyl hyperreactivity that is less pronounced than for longer A/T-tracts, but which is still significantly stronger than for "random" sequence DNA

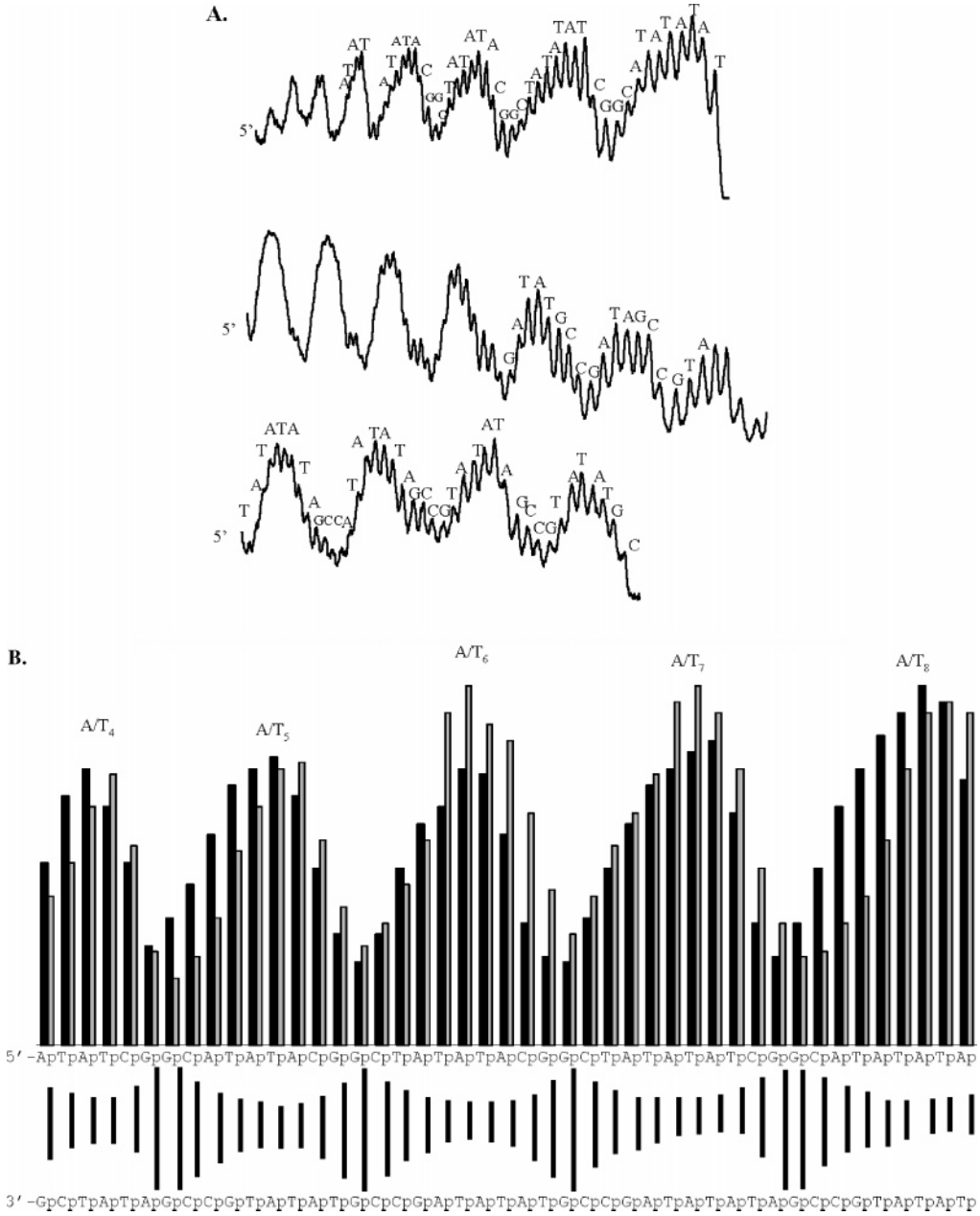

FIGURE 4: Uranyl photocleavage of A/T-rich sequences from pTA_{1-8}. (A) Results are represented by scans for both strands obtained by labeling in the 3′ end. (B) Correlation between calculated uranyl phosphate binding and minor groove width in the TA-tracts. The histogram shows calculated uranyl binding to the *n*th (black bars) (using Y_n and Y_{n+1}) and the $(n - 2)$th (gray bars) phosphates. Uranyl binding is correlated with the width of the minor groove as in Figure 1. Because the results for the A and T strands were obtained from different experiments, the absolute cleavage/binding efficiencies cannot be compared accurately.

(Figure 4A). Therefore, uranyl appears to be sensing some other structural/dynamic feature of the DNA in addition to minor groove width. Most likely this feature is connected to DNA helix flexibility/deformability that would allow minor groove compression (*vide infra*). In terms of flexibility, T/G steps could show similar behavior, but analyses of the DNA fragments in the present study as well as of data from previous studies indicate that this is not the case. However, a dedicated study to address the issue could be warranted.

Uranyl Photocleavage of A_4T_4 and T_4A_4 Exhibits the Presence of an Unusual A-Tract Structure in Both Sequences. Several experimental approaches have been designed to study why 5′-$A_4T_4N_2$ multimers migrate anomalously slowly in gels, indicating a curved structure, whereas multimers of the analogous 5′-$T_4A_4N_2$ migrate like normal B DNA of the same length characteristic for a noncurved structure (*43*).

Two plasmids containing the symmetrical sequences 5′-CGAAAATTTTCG (pA_4T_4) or 5′-CGTTTTAAAACG (pT_4A_4) were constructed to address this issue. In Figure 5, the uranyl cleavage patterns of the two DNA fragments (each containing four repeats) are compared.

The 5′-CGAAAATTTTCG sequence exhibits significant position variations in uranyl cleavage. Cleavage is increasing from the 5′ end of the four adenines toward the 3′ end, where the strong reactivity continues through the 5′-AT step into the four thymidines with a maximum at the 3′ end. This indicates that the 5′-AT step does not affect a continuous build up of the A-tract structure toward the 3′ end (parts A and B of Figure 5, upper scan). In fact, the pattern is

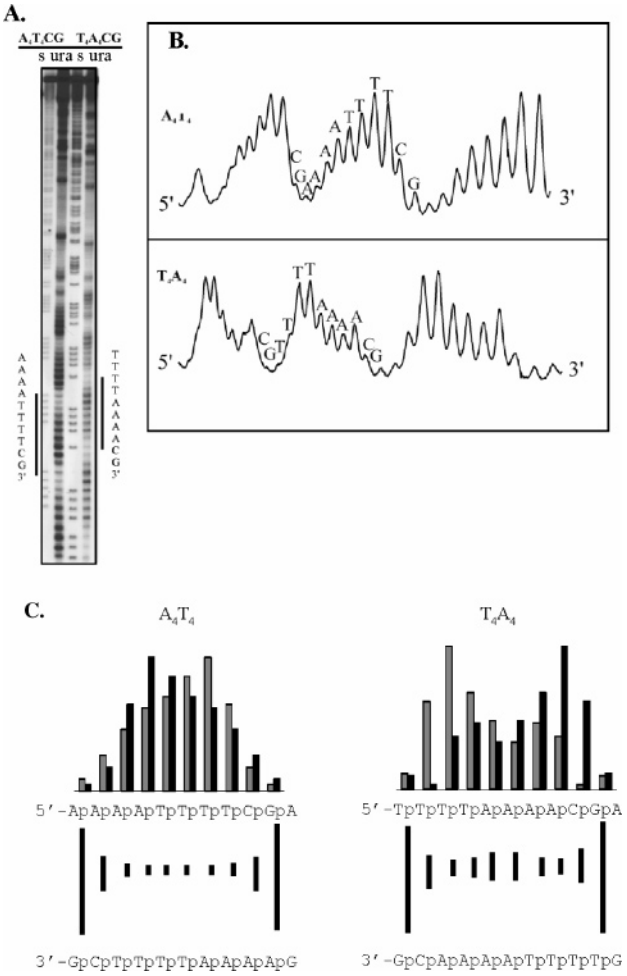

FIGURE 5: Uranyl photocleavage of $(CGAAAATTTTCG)_4$ and $(CGTTTTAAAACG)_4$ sequences. The results are represented with autoradiogram (A) and scans (B). Two lanes, one with a A/G sequence (s) and one with the uranyl cleavage reaction (ura), are shown for each sequence in the autoradiogram (A). The sequences are indicated for one repeat for each sequence in the scans (B). (C) Correlation between calculated uranyl phosphate binding and minor groove width in $(CGAAAATTTTCG)_4$ and $(CGTTTTAAAACG)_4$ sequences. The histogram shows calculated uranyl binding to the *n*th (black bars) (using Y_n to Y_{n-3} and Y_{n+1} to Y_{n+4}) and the $(n - 2)$th (gray bars) phosphates. Uranyl binding is correlated with the width of the minor groove as in Figure 1. The results for the A and T strands were obtained from cleavage on the same DNA fragment experiments, and therefore, the absolute cleavage/binding efficiencies can be compared directly.

reminiscent of the cleavage of the pure A_8-tract (see Figure 1B). Interestingly, the uranyl cleavage of the 5′-CGTTTTAAAACG sequence is fundamentally different. Reactivity is gradually increasing from the 5′ end toward the 3′ end of the four thymidines, whereas a more uniform and much weaker cleavage is observed at the four adenines, with adenine number three from the 5′ end showing the weakest cleavage (Figure 5B, lower scan). This shows that the structure of this nonbent sequence is different from both random DNA and pure A-tracts and that the TA step has a very strong effect on uranyl cleavage and thus on the DNA structure.

When cleavage intensities are aligned with the sequence (Figure 5C), cleavage at opposite strands is not correlated over the minor groove for either the A_4T_4 or the T_4A_4 sequences, which clearly indicates structures different from

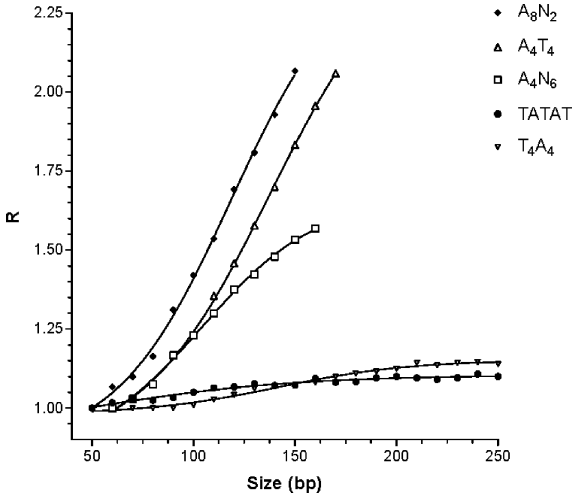

FIGURE 6: Comparison of *R* values for A_4N_6, A_4T_4,T_4A_4, TATAT, and A_8N_2 sequences. A quantitative measure of anomalous gel mobility was obtained by plotting the *R* values versus the actual size of the DNA fragment (*R* is the apparent chain length of a certain DNA fragment as judged by its migration compared to a standard DNA fragment of normal mobility divided by the actual chain length of the fragment).

that of an A_8-tract. Nonetheless, a gel-migration analysis reveals that $A_4T_4N_2$ migrates more like A_8N_2 than A_4N_6, indicating that A_4T_4 may structurally to some extent resemble an A_8-tract in terms of DNA bending (Figure 6). As expected, the 5′-$T_4A_4N_2$ multimers do not show anomalous migration. It is also clear that the uranyl photocleavage of both the unbent 5′-T_4A_4 and the bent 5′-A_4T_4 domain is unusual and fundamentally different from the cleavage of A-tracts, TA-tracts, and random DNA in being highly asymmetric between close phosphates across the minor groove. This asymmetry could be due to asymmetry in the binding of the uranyl relative to the two phosphates. Accepting this interpretation and using the combined cleavage information of both the *n*th and the $(n - 2)$th position, one may still obtain an estimated measure of uranyl affinity for a particular site in the minor groove. Such an analysis reveals that, whereas the minor groove structure is smoothly narrowing through the 5′-AT step in the 5′-A_4T_4 sequence, a distinct change is present around the 5′-TA step of the 5′-T_4A_4 sequence, essentially dividing this into two separate structural domains (Figure 5C). The reason uranyl would bind asymmetrically in the minor groove of these helices is not clear and warrants further study.

CONCLUSION

There is compelling evidence in support of the contention that pure adenine tracts in curved DNA have a unique conformation clearly distinguished from that of normal B DNA. One important feature of this conformation is narrowing of the minor groove from the 5′ end toward the 3′ end induced by a cooperative build-up mechanism. This is reflected in a parallel increase in sensitivity to uranyl photocleavage. However, a similar effect is observed in TA-tracts. Indeed, the uranyl photocleavage patterns of a pure A-tract and a TA-tract are almost identical, which has been ascribed to a very similar minor groove width (*24*, *32*). However, this simple interpretation may not be the full explanation.

Not surprisingly, cations appear to play a pivotal role in inducing DNA structures and conformations such as A-tract conformations (*38*, *42*). Consequently, it may well be that under certain conditions the uranyl ion shifts the DNA structure equilibrium upon binding and that the strong cleavage in A/T-rich sequences (and in other sequences) in addition to average ("static") minor groove width could also reflect high DNA helix deformability or flexibility that facilitates uranyl coordination to the phosphates over the minor groove in these regions. This effect would be expected to be particularly pronounced at the highly deformable or flexible TA steps. Indeed, our results show that even single 5′-TA steps exhibit increased susceptibility toward uranyl photocleavage. Thus, uranyl photocleavage may probe a combination of a pre-existing (high occupancy or "static") helix structure and a readily inducible helix structure as previously suggested (*32*). In this respect, it would therefore ideally complement the hydroxyl radical cleavage, which solely probes the average structure in terms of solvent accessibility. For instance, this mechanism would explain why A-tracts are probed analogously by uranyl and hydroxyl radicals, whereas TA-tracts are only differentially recognized by uranyl. In other words, hydroxyl radicals would probe the appearance of the DNA helix, while the uranyl in addition would report flexibility properties, which could indeed be extremely relevant for understanding the binding of proteins (such as CRP or TBP) that perturb the DNA helix.

Furthermore, it is possible that the difference between A-tract and TA-tract structures and the bending properties of A-tracts may indeed reflect a difference in flexibility: A-tracts adopt a very rigid DNA structure in contrast to sequences containing the very flexible TA base pair step (*14*, *22*, *40*). Thus, TA-tracts may build up a flexible structure with a (readily inducible) narrow minor groove like in pure A-tracts. In addition, a single TA step is able to perturb the rigid A-tract structure by inducing local flexibility (and a slight local widening of the minor groove), which is sufficient to disrupt DNA curvature. Therefore, the present results support a model according to which bending would predominantly be a consequence of the rigid A-tract DNA region and its junction with adjacent more flexible DNA.

On the basis of this interpretation of our data, we would consider the most likely mechanism for binding of minor groove ligands (including uranyl(VI), other cations, as well as organic minor groove binders such as distamycin or Hoechst) to AT sequences as predominantly an induced fit by which the groove binder upon binding modifies the minor groove conformation compatible with the various binding interactions (*45*−*47*).

Finally, our results suggest that both the bent A_4T_4 and the nonbent T_4A_4 sequences have unusual DNA structures that result in backbone asymmetry for uranyl binding. Nonetheless, the uranyl probing clearly distinguishes the two sequences, and our interpretation of the data is consistent with a structure for the bent A_4T_4 sequence that resembles a continuous A-tract (which consequently produces macroscopic bending), whereas the nonbent T_4A_4 sequences is closer to two independent and opposite A-tracts that cancel each other in terms of macroscopic bending. Again, the flexibility of the 5′-TA step would allow for formation of the two structurally independent domains.

In conclusion, rather than being solely a probe for average ("static") minor groove width, uranyl may additionally have the propensity of probing DNA flexibility/deformability, which has an important function in many biological processes such as folding of DNA in nucleosomes and chromatin as well as in induced fit of sequence-specific protein−DNA recognition. Furthermore, the results would indicate that A-tracts adopt a rigid helix conformation with a narrow minor groove, whereas the helix of AT-tracts has very high flexibility/deformability that readily allows for minor groove compression upon binding of certain cations such as UO_2^{2+} (and possibly Mg^{2+}) or minor groove binding drugs. As a consequence of this interpretation, macroscopic DNA bending would require a rigid A-tract, and the data will thus support the "junction model".

ACKNOWLEDGMENT

We thank Neel Louv-Jansen for expert technical assistance.

REFERENCES

1. Hagerman, P. J. (1990) Sequence-directed curvature of DNA, *Annu. Rev. Biochem. 59*, 755−781.
2. Ulanovsky, L. E., and Trifonov, E. N. (1987) Estimation of wedge components in curved DNA, *Nature 326*, 720−722.
3. Trifonov, E. N., and Sussman, J. L. (1980) The pitch of chromatin DNA is reflected in its nucleotide sequence, *Proc. Natl. Acad. Sci. U.S.A. 77*, 3816−3820.
4. Goodsell, D. S., Kaczor-Grzeskowiak, M., and Dickerson, R. E. (1994) The crystal structure of C−C−A−T−T−A−A−T−G−G. Implications for bending of B-DNA at T−A steps, *J. Mol. Biol. 239*, 79−96.
5. Grzeskowiak, K., Goodsell, D. S., Kaczor-Grzeskowiak, M., Cascio, D., and Dickerson, R. E. (1993) Crystallographic analysis of C−C−A−A−G−C−T−T−G−G and its implications for bending in B-DNA, *Biochemistry 32*, 8923−8931.
6. Wu, H. M., and Crothers, D. M. (1984) The locus of sequence-directed and protein-induced DNA bending, *Nature 308*, 509−513.
7. Koo, H.-S., Wu, H.-M., and Crothers, D. M. (1986) DNA bending at adenine.thymine tracts, *Nature 320*, 501−506.
8. Koo, H.-S., Wu, H.-M., and Crothers, D. M. (1988) Calibration of DNA curvature and a unified description of sequence-directed bending, *Proc. Natl. Acad. Sci. U.S.A. 85*, 1763−1767.
9. Burkhoff, A. M., and Tullius, T. D. (1987) The unusual conformation adopted by the adenine tracts in kinetoplast DNA, *Cell 48*, 935−943.
10. MacDonald, D., Herbert, K., Zhang, X., Pologruto, T., Lu, P., and Polgruto, T. (2001) Solution structure of an A-tract DNA bend, *J. Mol. Biol. 306*, 1081−1098.
11. Katahira, M., Sugeta, H., and Kyogoku, Y. (1990) A new model for the bending of DNAs containing the oligo(dA) tracts based on NMR observations, *Nucleic Acids Res. 18*, 613−618.
12. Leroy, J. L., Charretier, E., Kochoyan, M., and Gueron, M. (1988) Evidence from base-pair kinetics for two types of adenine tract structures in solution: Their relation to DNA curvature, *Biochemistry 27*, 8894−8898.
13. Nadeau, J. G., and Crothers, D. M. (1989) Structural basis for DNA bending, *Proc. Natl. Acad. Sci. U.S.A. 86*, 2622−2626.
14. Nelson, H. C., Finch, J. T., Luisi, B. F., and Klug, A. (1987) The structure of an oligo(dA).oligo(dT) tract and its biological implications, *Nature 330*, 221−216.
15. Digabrielle, A. D., Sanderson, M. R., and Steitz, T. A. (1993) A DNA dodecamer containing an adenine tract crystallizes in a unique lattice and exhibits a new bend, *J. Mol. Biol. 231*, 1024−1039.
16. Chuprina, V. P. (1987) Anomalous structure and properties of poly(dA).poly(dT). Computer simulation of the polynucleotide structure with the spine of hydration in the minor groove, *Nucleic Acids Res. 12*, 293−311.
17. Kopka, M. L., Fratini, A. V., Drew, H. R., and Dickerson, R. E. (1983) Ordered water structure around a B-DNA dodecamer. A quantitative study, *J. Mol. Biol. 163*, 129−146.

18. Coll, M., Frederick, C. A., Wang, A. H., and Rich, A. (1987) A bifurcated hydrogen-bonded conformation in the d(A.T) base pairs of the DNA dodecamer d(CGCAAATTTGCG) and its complex with distamycin, *Proc. Natl. Acad. Sci. U.S.A. 84*, 8385−8389.
19. Dickerson, R. E., and Drew, H. R. (1981) Structure of a B-DNA dodecamer. II. Influence of base sequence on helix structure, *J. Mol. Biol. 149*, 761−786.
20. Edwards, K. J., Brown, D. G., Spink, N., Skelly, J. V., and Neidle, S. (1993) Molecular structure of the B-DNA dodecamer d(CG-CAAATTTGCG)2. An examination of propeller twist and minor-groove water structure at 2.2 Å resolution, *J. Mol. Biol. 20*, 1161−1173.
21. Møllegaard, N. E., Bailly, C., Waring, M. J., and Nielsen, P. E. (1997) Effects of diaminopurine and inosine substitutions on A-tract induced DNA curvature. Importance of the 3′−A-tract junction, *Nucleic Acids Res. 25*, 3497−3502.
22. Yoon, C., Prive, G. G., Goodsell, D. S., and Dickerson, R. E. (1988) Structure of an alternating-B DNA helix and its relationship to A-tract DNA, *Proc. Natl. Acad. Sci. U.S.A. 85*, 6332−6336.
23. Johannesson, H., and Halle, B. (1998) Minor groove hydration of DNA in solution: Dependence on base composition and sequence, *J. Am. Chem. Soc. 120*, 6859−6870.
24. Sonnichsen, S. H., and Nielsen, P. E. (1996) Enhanced uranyl photocleavage across the minor groove of all (A/T)4 sequences indicates a similar narrow minor groove conformation, *J. Mol. Recognit. 9*, 219−227.
25. Jeppesen, C., and Nielsen, P. E. (1989) Uranyl mediated photofootprinting reveals strong *E. coli* RNA polymerase−DNA backbone contacts in the +10 region of the DeoP1 promoter open complex, *Nucleic Acids Res. 17*, 4947−4956.
26. Møllegaard, N. E., Rasmussen, P. B., Valentin-Hansen, P., and Nielsen, P. E. (1993) Characterization of promoter recognition complexes formed by CRP and CytR for repression and by CRP and RNA polymerase for activation of transcription on the *Escherichia coli* deoP2 promoter, *J. Biol. Chem. 268*, 17471−17477.
27. Møllegaard, N. E., Murchie, A. I., Lilley, D. M., and Nielsen, P. E. (1994) Uranyl photoprobing of a four-way DNA junction: Evidence for specific metal ion binding, *EMBO J. 13*, 1508−13.28.
28. , Møllegaard, N. E., and Nielsen, P. E. (1997) Uranyl photoprobing of DNA structures and drug−DNA complexes, *Methods Mol. Biol. 90*, 43−49.
29. Bassi, G. S., Møllegaard, N. E., Murchie, A. I., von Kitzing, E., and Lilley, D. M. (1995) Ionic interactions and the global conformations of the hammerhead ribozyme, *Nat. Struct. Biol. 2*, 45−55.
30. Nielsen, P. E., Mollegaard, N. E., and Jeppesen, C. (1990) DNA conformational analysis in solution by uranyl mediated photocleavage, *Nucleic Acids Res.* 1990 Jul 11;18(13):3847−3851.
31. Nielsen, P. E., Hiort, C., Sonnichsen, S. H., Buchardt, O., Dahl, O., and Norden, B. (1992) DNA binding and photocleavage by uranyl(VI)(UO_2^{2+}) salts, *J. Am. Chem. Soc. 114*, 4967−4975.
32. Møllegaard, N. E., and Nielsen, P. E. (2003) Increased temperature and 2-methyl-2,4-pentanediol change the DNA structure of both curved and uncurved adenine/thymine-rich sequences, *Biochemistry 42*, 8587−8593.
33. Chuprina, V. P., Fedoroff, O. Y., and Reid, B. R. (1991) New insights into the structure of An tracts and B′−B′ bends in DNA, *Biochemistry 30*, 561−568.
34. Katahira, M., Sugeta, H., and Kyogoku, Y. (1990) Determination of the conformation of d(GGAAATTTCC)2 in solution by use of ^{1}H NMR and restrained molecular dynamics, *Biochemistry 29*, 7214−7222.
35. Haran, T. E., and Crothers, D. M. (1989) Cooperativity in A-tract structure and bending properties of composite T*n*A*n* blocks, *Biochemistry 28*, 2763−2767.
36. Hagerman, P. J. (1985) Sequence dependence of the curvature of DNA: A test of the phasing hypothesis, *Biochemistry 24*, 7033−7037.
37. Mack, D. R., Chiu, T. K., and Dickerson, R. E. (2001) Intrinsic bending and deformability at the T−A step of CCTTTAAAGG: A comparative analysis of T−A and A−T steps within A-tracts, *J. Mol. Biol. 312*, 1037−1049.
38. Hud, N. V., Sklenar, V., and Feigon, J. (1999) Localization of ammonium ions in the minor groove of DNA duplexes in solution and the origin of DNA A-tract bending, *J. Mol. Biol. 286*, 651−660.
39. Burkhoff, A. M., and Tullius, T. D. (1988) Structural details of an adenine tract that does not cause DNA to bend, *Nature 331*, 455−457.
40. Goodsell, D. S., Kaczor-Grzeskowiak, M., and Dickerson, R. E. (1994) The crystal structure of C−C−A−T−T−A−A−T−G−G. Implications for bending of B-DNA at T−A steps, *J. Mol. Biol. 239*, 79−96.
41. Quintana, J. R., Grzeskowiak, K., Yanagi, K., and Dickerson, R. E. (1992) Structure of a B-DNA decamer with a central T−A step: C−G−A−T−T−A−A−T−C−G, *J. Mol. Biol. 225*, 379−395.
42. Liepinsh, E., Leupin, W., and Otting, G. (1994) Hydration of DNA in aqueous solution: NMR evidence for a kinetic destabilization of the minor groove hydration of d-(TTAA)2 versus d-(AATT)2 segments, *Nucleic Acids Res. 22*, 2249−2254.
43. Hagerman, P. J. (1986) Sequence-directed curvature of DNA, *Nature 321*, 449−450.
44. Hud, N. V., and Feigon, J. (2002) Characterization of divalent cation localization in the minor groove of the A(*n*)T(*n*) and T(*n*)A(*n*) DNA sequence elements by ^{1}H NMR spectroscopy and manganese(II), *Biochemistry 41*, 9900−9910.
45. McFail-Isom, L., Sines, C. C., and Williams, L. D. (1999) DNA structure: Cations in charge? *Curr. Opin. Struct. Biol. 9*, 298−304.
46. Laughton, C., and Luisi, B. (1999) The mechanics of minor groove width variation in DNA, and its implications for the accommodation of ligands, *J. Mol. Biol. 288*, 953−963.
47. Bostock-Smith, C. E., Harris, S. A., Laughton, C. A., and Searle, M. A. (2001) Induced fit DNA recognition by a minor groove binding analogue of Hoechst 33258: Fluctuations in DNA A tract structure investigated by NMR and molecular dynamics simulations, *Nucleic Acids Res. 29*, 693−702.

BI0502083